

# Tomographic optical breast imaging guided by three-dimensional mammography

Ang Li, Eric L. Miller, Misha E. Kilmer, Thomas J. Brukilacchio, Tina Chaves, Jonathan Stott, Quan Zhang, Tao Wu, MaryAnn Chorlton, Richard H. Moore, Daniel B. Kopans, and David A. Boas

We introduce a modified Tikhonov regularization method to include three-dimensional x-ray mammography as a prior in the diffuse optical tomography reconstruction. With simulations we show that the optical image reconstruction resolution and contrast are improved by implementing this x-ray-guided spatial constraint. We suggest an approach to find the optimal regularization parameters. The presented preliminary clinical result indicates the utility of the method. © 2003 Optical Society of America  
OCIS codes: 170.6960, 170.5280, 170.3830, 170.3010, 170.3880, 170.0110.

## 1. Introduction

The development of diffuse optical tomography (DOT) to obtain three-dimensional (3-D) images of the spatially varying absorption and scattering properties of highly scattering media probed by near infrared light has advanced rapidly during the past decade.<sup>1-3</sup> Its clinical application to imaging breast cancer and brain pathology and activity<sup>4-8</sup> is beginning to show more promise as preliminary clinical results begin to demonstrate the feasibility of extracting physiologically relevant information from the images reconstructed from the diffuse optical measurements. As the inverse imaging problem for DOT is ill-conditioned and generally underdeter-

mined, the image quality is compromised by poor spatial resolution and sensitivity to measurement noise.<sup>2</sup> This can be improved modestly by optimization of the geometry and number of measurements,<sup>9</sup> but significant improvement will be obtained by including prior information in the image reconstruction.

Previously researchers have tried different ways to combine *a priori* structural information from magnetic resonance imaging (MRI)<sup>10,11</sup> or ultrasound (US)<sup>12</sup> into the DOT reconstruction procedure. The most straightforward way is to assume that optical perturbation comes mostly from the region of interest (ROI) shown in the US; MRI, or x-ray structural images. In this case, the DOT image reconstruction is limited just to the ROI, which makes for a particularly simple imaging problem since the sensitivity matrix needs to be calculated only over this small area.<sup>13</sup> A second method divides the whole medium into different types of tissue (fat, glandular tissue, tumor, etc), and each tissue type is homogeneous and has its own optical properties.<sup>13</sup> In this way the number of unknowns is greatly reduced and the speed of the image reconstruction is increased. Both methods have the disadvantage that the geometric assumptions are too rigidly enforced in the DOT image formation process. Specifically, errors in the boundaries identified by x-ray, MRI, or US lead to strongly biased results in the resulting DOT image.

Motivated by this shortcoming, we describe an alternative approach in which the contrast seen in the MRI, x-ray, or US images are assumed to be proportional to the DOT contrast. A linear least-squares type of DOT image formation problem is then posed

---

A. Li (angli@nmr.mgh.harvard.edu) is with the Department of Physics, Tufts University, Medford, Massachusetts 02155. A. Li, along with T. J. Brukilacchio, T. Chaves, J. Stott, Q. Zhang, and D. A. Boas, is also with the Athinoula A. Martinos Center for Biomedical Imaging, Massachusetts General Hospital, Harvard Medical School, Charlestown, Massachusetts 02129. E. L. Miller is with the Department of Electrical and Computer Engineering, Northeastern University, Boston, Massachusetts 02115. M. E. Kilmer is with the Department of Mathematics, Tufts University, Medford, Massachusetts 02155. T. J. Brukilacchio is also with the Department of Electrical Engineering, Tufts University, Medford, Massachusetts 02155. T. Wu, M. A. Chorlton, R. H. Moore, and D. B. Kopans are with the Breast Imaging Unit, Massachusetts General Hospital, Harvard Medical School, Boston, Massachusetts 02114.

Received 4 February 2003; revised manuscript received 19 May 2003.

0003-6935/03/255181-10\$15.00/0

© 2003 Optical Society of America

in which the cost function comprises two terms: the normal data residual term and a second term that encompasses this structural information. The advantage of this method is that one can adjust the influence of the structural information by appropriately weighting the structural component of the cost function.

The key challenge with our method is the development of a useful approach for choosing multiple optimal regularization parameters. Methods for space-varying regularization have been considered in a number of contexts in the recent past including DOT<sup>14</sup> and geophysical exploration.<sup>15</sup> Both methods are appropriate for problems in which the parameter is smoothly varied over a region of space. Our method is a bit different because we wish to choose one parameter for the ROI and a second for the rest of space: This multiple regularization parameter problem is not well studied; see, e.g., Ref. 16 for an overview. Here we explore a hybrid method that combines the L-curve approach for finding one parameter with a signal-to-noise ratio (SNR)-type of maximization for the second.

In Section 2 we present a formulation for implementing this prior spatial constraint into the DOT problem. In Sections 3, 4, and 5 we present simulation results that indicate the utility of this spatial constraint and the methodology for choosing optimal regularization parameters. Finally, in Section 6 we demonstrate the use of the method on simultaneously acquired clinical 3-D x-ray mammography and optical breast imaging data. We believe that this multimodality approach will allow DOT to enter into the screening and diagnostic breast imaging arena by allowing functional (provided by the optical absorption/scattering spectroscopy) interpretation of the x-ray structural images, potentially leading to improved sensitivity and specificity over x-ray alone. Our simulation results show that the contrast and resolution of diffuse optical images could be improved in the presence of high noise given the soft structural constraint provided by a 3-D x-ray mammogram.

## 2. Theory

The formulation of the forward and inverse problem for DOT is well documented in the literature.<sup>2,13</sup> The soft constraint is incorporated into the linearized DOT problem through minimization of the objective function  $f(\mathbf{x})$ :

$$f(\mathbf{x}) = \|\mathbf{y} - A\mathbf{x}\|^2 + \lambda_1\|(I - S)\mathbf{x}\|^2 + \lambda_2\|S\mathbf{x}\|^2. \quad (1)$$

The optical image to be reconstructed is indicated by  $\mathbf{x}$ , the system matrix is given by  $A$ , which is the projection from the image domain to the measurement domain;  $\mathbf{y}$  is a vector of the optical measurement data;  $I$  is the identity matrix; and  $S$  is a diagonal matrix, the diagonal of which describes the hypothesized support of the tumor as indicated by the x-ray image. More specifically, in discrete form, the  $i$ th element of the diagonal is a 1 if the  $i$ th voxel is identified as part of the tumor by the x-ray image and

0 otherwise.  $\lambda_1$  and  $\lambda_2$  are the two regularization parameters that control the degree of regularization in the background and lesion, respectively. This objective function has three separate terms: the residual between the optical measurement and the theoretical estimate of the measurement, the norm of the image whose pixels are not selected by a structural/spatial prior and thus are suspected of having weak optical contrast (i.e.,  $\lambda_1$  is large), and the norm of the image whose pixels are selected by the structural prior and thus are suspected of having strong optical contrast (i.e.,  $\lambda_2$  is smaller). Note that, if  $\lambda_2$  is set equal to  $\lambda_1$ , the formulation is reduced to the conventional Tikhonov regularization scheme.

The minimization of Eq. (1) is given by

$$\mathbf{x} = [A^T A + \Lambda(\mathbf{r})]^{-1} A^T \mathbf{y}. \quad (2)$$

In the conventional Tikhonov regularization scheme,  $\lambda$  is a scalar. Here,  $\lambda(\mathbf{r})$  is allowed to vary spatially across the pixels of the image and is derived from the  $\lambda_1$  and  $\lambda_2$  in Eq. (1). This type of spatial regularization for DOT was first introduced by Arridge and Sehueiger<sup>17</sup> and elaborated by Pogue *et al.*<sup>14</sup> When  $\mathbf{r}$  is within the pixels having low lesion probability as indicated in matrix  $S$  (region 1),  $\lambda(\mathbf{r})$  will be assigned  $\lambda_1$ . When  $\mathbf{r}$  is within the pixels having a high lesion probability (region 2),  $\lambda(\mathbf{r})$  will have the smaller value  $\lambda_2$ . That is,

$$\lambda(\mathbf{r}) = \begin{cases} \lambda_1 & \text{if } \mathbf{r} \text{ is in region 1} \\ \lambda_2 & \text{if } \mathbf{r} \text{ is in region 2} \end{cases}$$

A smaller value for  $\lambda(\mathbf{r})$  reduces the penalty for the reconstruction of optical contrast and thus increases the probability of finding contrast in the designated region. Unfortunately, it will also increase the image noise in the designated region. We explore the trade-off between these factors while searching for the optimal regularization parameters. The formulation presented in Eq. (2) is easily modified to handle a soft structural constraint from a 3-D image from x-ray computed tomography, MRI, or US.

## 3. Simulation Results

Simulations were performed to explore the improvement in DOT image performance with prior spatial information incorporated by use of this spatial regularization scheme. Transillumination through a 6-cm slab was simulated. The optical properties were  $\mu_a = 0.05 \text{ cm}^{-1}$  and  $\mu_s' = 5 \text{ cm}^{-1}$  for the absorption and reduced scattering coefficient, respectively. A spherical heterogeneity with a radius of 1 cm and  $\mu_a = 0.1 \text{ cm}^{-1}$  and  $\mu_s' = 5 \text{ cm}^{-1}$  was positioned in the center of the otherwise homogeneous medium [see Fig. 1(a)]. Sixteen sources and 16 detectors were positioned on opposing  $4 \times 4$  grids with a 2-cm spacing to collect transmitted data. The modulation frequency of the laser sources was 200 MHz. Electronic noise and photon shot noise were added to the simulated measurements generated by the first Born approximation for an absorbing heterogeneity in a slab geometry.<sup>18</sup> The amplitude SNR

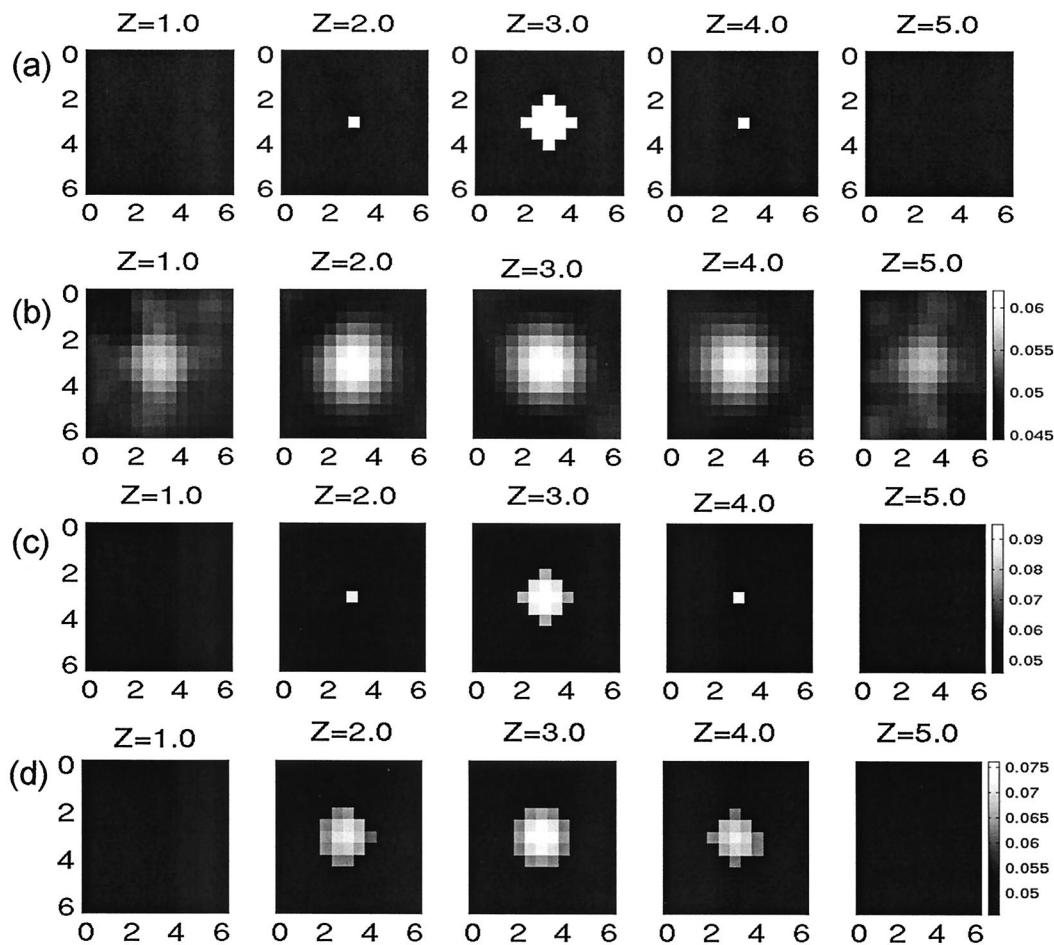


Fig. 1. (a) Absorption anomaly to be reconstructed. (b) Absorption image reconstruction of simulated data by use of conventional Tikhonov regularization (image units are in reciprocal centimeters). (c) Image reconstructed with a spatial prior for the regularization. The spatial prior has the correct spatial information for the location of the heterogeneity. (d) Image reconstructed with the original optical image in (b) as a spatial prior, as described in the text. The field of view of the image is  $6\text{ cm} \times 6\text{ cm}$ , and image slices are shown every centimeter.

ranged from 30 to 80 dB (or approximately 0.01% to 10%) across different source–detector pairs and the phase noise varied between 0.2 and 2 deg.<sup>19–21</sup> The tomographic optical images were reconstructed by use of the Rytov approximation. Both the conventional Tikhonov regularization ( $\lambda_1 = \lambda_2$ ) and the spatial prior Tikhonov regularization ( $\lambda_2 < \lambda_1$ ) were used to solve the inverse problem. For the spatial prior, we collocated the position of the optical contrast and the 3-D x-ray structural contrast. That is, the region regularized by  $\lambda_2$  is exactly the region with the true optical contrast. For the regularization parameters we used values of  $\lambda_n = \alpha_n \max(A^T A)$  with  $\alpha_1 = 0.5$  and  $\alpha_2 = 0.06$ . From a comparison of the reconstructions of the absorption perturbation we see clearly the improved resolution, contrast accuracy, and contrast-to-noise ratio (CNR) in the reconstruction with the spatial prior [see Figs. 1(b) and 1(c)]. In Fig. 1(d) we show a different kind of spatial prior result when we obtained the prior by thresholding the optical image shown in Fig. 1(b) halfway between the background value and the peak contrast value. This type of spatial prior might have some advantage

when structural information cannot be provided by another imaging modality. Note that the resolution of Fig. 1(d) is not as good as when we used the higher resolution spatial prior in Fig. 1(c). Here we reconstruct only the absorption perturbation image, assuming that the scattering coefficient is spatially uniform.

To study the effect of variation of the  $\alpha_1$ ,  $\alpha_2$  regularization parameters on the quality of the image reconstruction, we first introduce a few objective measures. The contrast-to-background noise ratio (CBNR) is defined as the ratio of the mean value of the image in the  $\alpha_2$  region to the mean image standard deviation in the  $\alpha_1$  region arising from the simulated measurement noise. The contrast-to-object noise ratio (CONR) is defined as the ratio of the mean value of the image in the  $\alpha_2$  region to the mean image standard deviation in the  $\alpha_2$  region. We introduce the full width at half-maximum (FWHM) of the object imaged along the axial direction and along the lateral direction to describe the resolution of the image.

The CBNR and the CONR are shown in Figs. 2(a) and 2(b) versus  $\alpha_2$  for a fixed  $\alpha_1$  (i.e.,  $\alpha_1 = 0.7$ ). Note

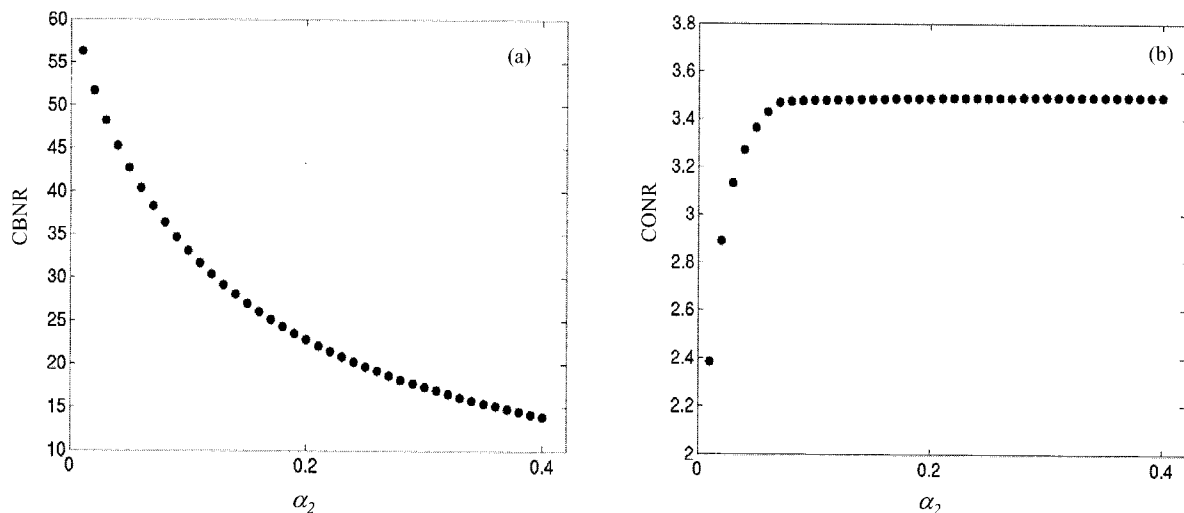


Fig. 2. Plot of objective measures of the reconstructed images versus regularization parameter  $\alpha_2$ . (a) CBNR versus  $\alpha_2$ , and (b) CONR versus  $\alpha_2$ .

that  $\alpha_2$  will always be less than  $\alpha_1$  so as to impose less regularization on the region of interest. Generally, with increasing  $\alpha_2$  the CBNR decreases and the CONR increases. Thus a balance must be found between CBNR and CONR. It is important to note that decreasing  $\alpha_2$  relative to  $\alpha_1$  can significantly increase the CBNR before causing an appreciable decrease in the CONR. The axial FWHM and lateral FWHM are shown in Fig. 3(a) and 3(b) and show the expected result of a smaller regularization parameter resulting in a smaller FWHM. The  $\alpha_2$  regularization parameter has a more significant effect on the axial resolution than on the lateral resolution, as is expected for a transmission measurement that generally laterally localizes an object well. Without the spatial prior, i.e.,  $\alpha_1 = \alpha_2$ , the CBNR  $\approx$  CONR  $\approx$  3.6, and the FWHM = 3.1 and 2.5 cm along the axial and lateral directions, respectively.

#### 4. Choosing the Optimal Regularization Parameters

We have shown that a spatial prior can improve the contrast and resolution of the reconstructed image. We next explore a method to choose optimal regularization parameters objectively. The procedure is composed of two steps. First, we use the L-curve technique<sup>20,22,23</sup> to determine  $\alpha_1$ . In this step,  $\alpha_2$  is kept equal to  $\alpha_1$ . The L-curve technique is an *a posteriori* method that uses only the measurement and the forward model. It can be applied to select the value of the regularization parameter that balances the trade-off between the minimization of the measurement residual and the minimization of the image noise. To create the L curve, we parametrically plot the log of the image norm  $\|x\|$  versus the log of the measurement residual as a function of  $\alpha_1$  [see Fig. 4(a)]. The arrow in Fig. 4(a) points to the so-

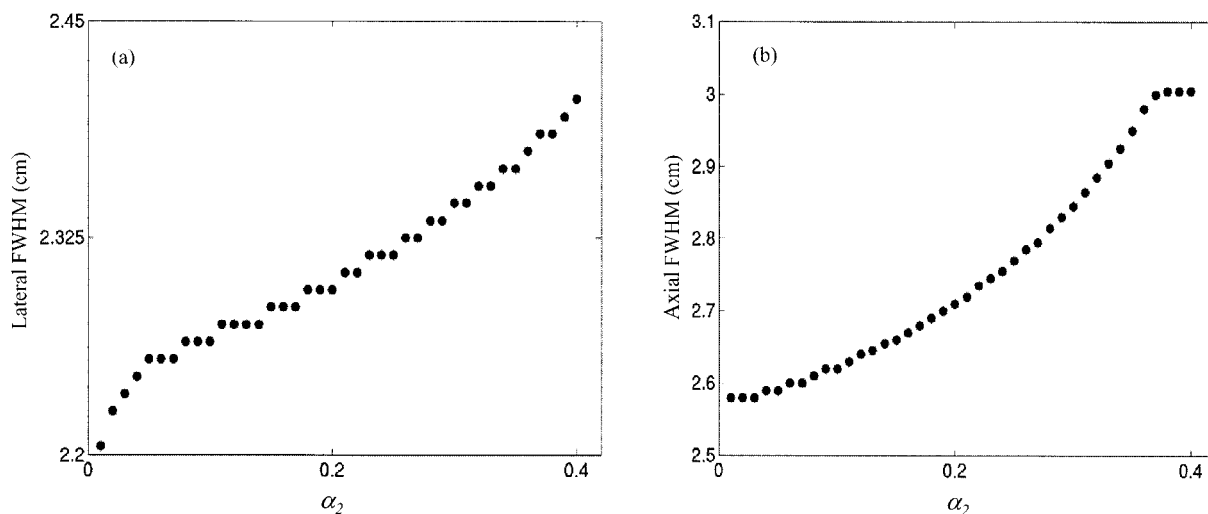


Fig. 3. Plot of the FWHM of the reconstructed absorbing heterogeneity in the (a) lateral and (b) axial directions versus regularization parameter  $\alpha_2$ .

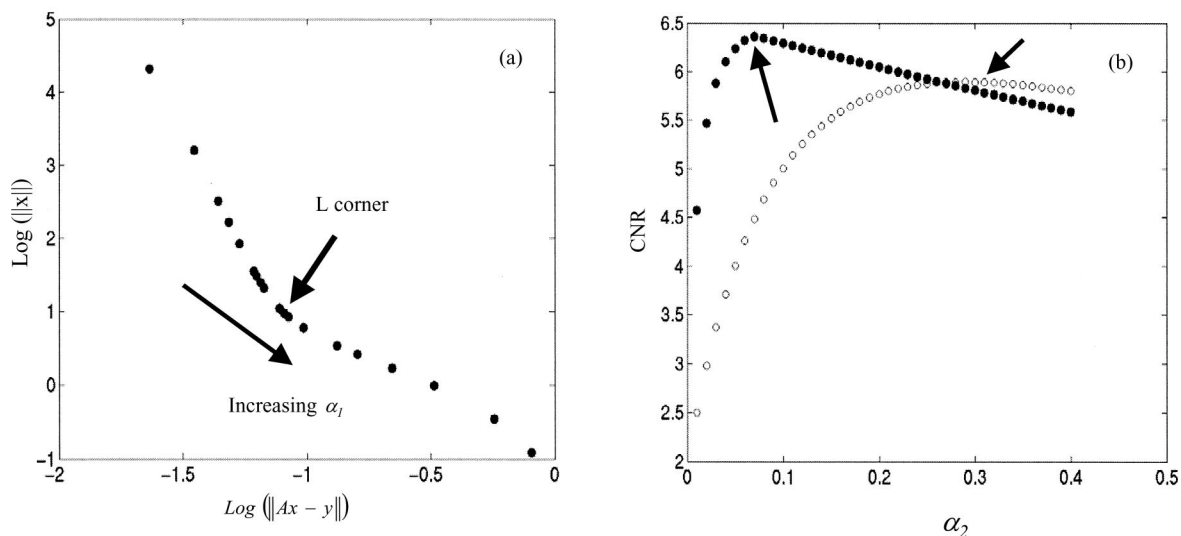


Fig. 4. (a) Plot of the L curve for the Tikhonov regularization reconstructed in Fig. 1(a). Here  $\alpha_2$  has the same value as  $\alpha_1$ . The arrows point to the L corner and indicate the direction of increasing  $\alpha_1$ . (b) CNR versus  $\alpha_2$ .  $\alpha_1 = 0.7$  remains constant at the value determined in (a). The arrows point to the maximum CNR. The filled circles indicate the CNR for the x-ray constraint. The open circles indicate the CNR when the optical image is used as the spatial constraint.

called L corner, the value at which  $\alpha_1$  is said to be optimal. Next we find an appropriate  $\alpha_2$  to impose the x-ray constraint. Here we need to find a compromise between two competing factors: (1) high resolution and contrast, and (2) increasing image noise. To do so, we plot CNR versus  $\alpha_2$ , where  $\text{CNR} = 2/(1/\text{CBNR} + 1/\text{CONR})$ . The  $\alpha_2$  that maximizes the CNR function is a good choice [see Fig. 4(b)].

### 5. Misalignment between the Optical and the X-Ray Contrast

In our previous simulations we assumed that the optical contrast is well correlated with the x-ray contrast (i.e., that the contrasts are aligned). Yet the actual correlation between optical and x-ray contrast is still unexplored. Therefore, it is possible that these two are only partially correlated or in fact uncorrelated. An example of this is shown in Figs. 5(a) and 5(b), in which the x-ray and optical contrast centers are laterally displaced by 3 cm and both have a 1-cm radius. We see that the optical contrast is reconstructed in the correct lateral position but that greater image noise is apparent in the position of the x-ray prior owing to the reduced regularization in that region for the CNR method described above we chose an optimal value of  $\alpha_2 = 0.05$ ). In this case the image resolution is comparable with the case of no spatial prior as shown in Fig. 1(b), since the spatial prior provides information inconsistent with the optical data. This inconsistent prior should act to bias the optical reconstruction. Indeed, for simulations in which the optical and x-ray centroids are laterally displaced by less than 3 cm, we observed that the position of the optical contrast is incorrectly reconstructed toward the center of the x-ray prior.

Misalignment of the optical and the x-ray contrast

in the axial direction is difficult to resolve because of poor axial resolution when imaging through a slab with a transillumination geometry. An example of this is shown in Figs. 5(c) and 5(d), in which the x-ray and optical contrast centers are axially displaced by 2 cm and both have a 1-cm radius. The optical contrast is centered at  $z = 2.0$  cm, and the x-ray contrast is centered at  $z = 4.0$  cm. We observed that optical contrast is reconstructed in the correct lateral and axial positions but that the maximum is reconstructed axially toward the position of the x-ray prior. In this case, for the CNR method described above we chose an optimal value of  $\alpha_2 = 0.08$ .

### 6. Preliminary Clinical Result

For this tomographic optical breast imaging feasibility study we used a coregistered frequency-domain diffuse optical imaging system and a 3-D tomosynthesis x-ray mammography system.<sup>24</sup> We used a homodyne frequency-domain optical imaging system with 780-nm lasers modulated at 70 MHz. A time-division multiplexing scheme was applied to distribute the laser light to 40 source positions. Nine avalanche photodiodes detect the output light, and in-phase and quadrature-phase demodulation convert the detected signal to amplitude and phase. In the tomosynthesis system, an amorphous Si-based flat panel detector locates in the same way as the film cassette in a conventional film-screen mammography system. It has  $1800 \times 2304$  pixels with a 100- $\mu\text{m}$  pixel size. Tomosynthesis reconstruction uses 11 projections taken over a  $50^\circ$  angular range above the base, with a  $5^\circ$  angular step.<sup>24,25</sup> The breast is compressed as in standard mammography. The probe is a combination of a standard x-ray compression plate and a removable optical fiber assembly. After the breast is appropriately positioned and compressed,

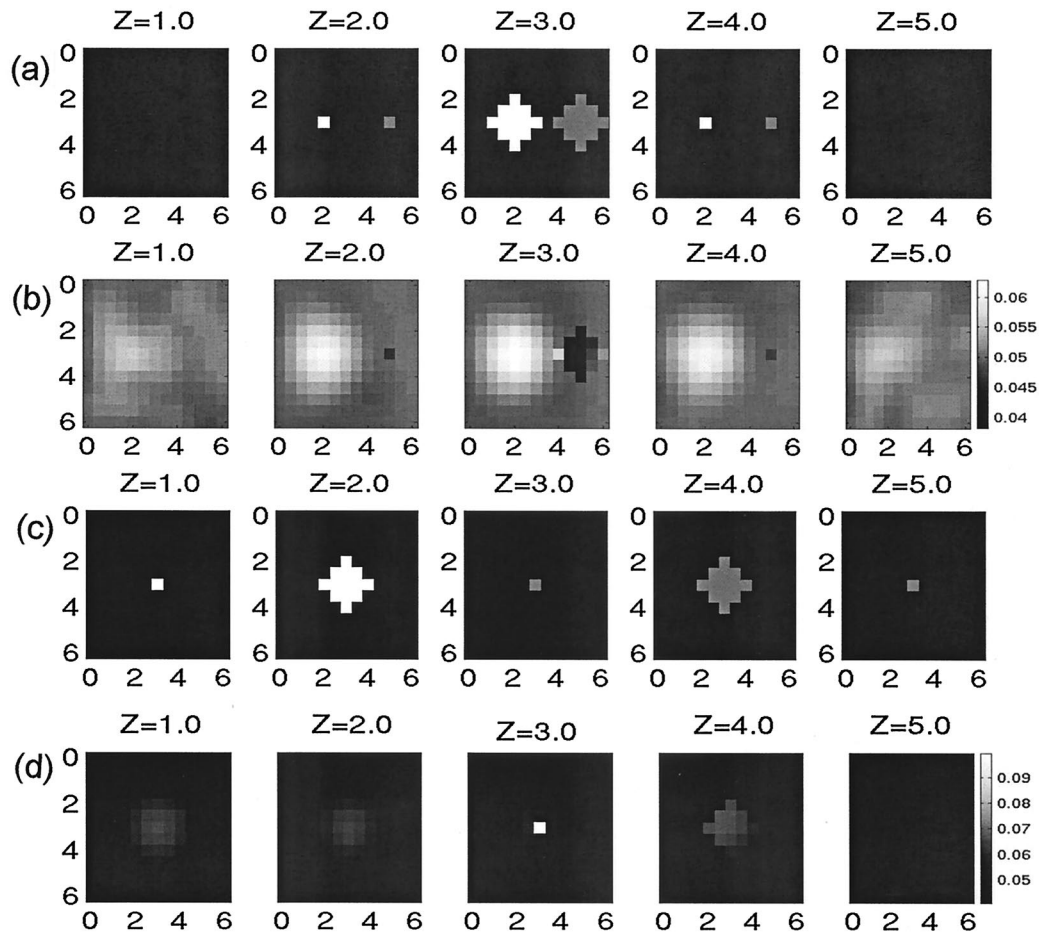


Fig. 5. Absorption image reconstruction of simulated data by use of an incorrect spatial prior in the lateral direction (image units are in reciprocal centimeters): (a) true target (white region) and ROI (gray region) and (b) reconstructed image. The centers of the spatial prior and the real object are displaced laterally by 3 cm along the  $x$  axis. The reconstruction of simulated data with an incorrect spatial prior in the axial direction: (c) true target (white) and ROI (gray) and (d) reconstructed image. The centers of the spatial prior and the real object are axially displaced by 2 cm along the  $z$  axis. The field of view of the image is  $6\text{ cm} \times 6\text{ cm}$ , and image slices are shown every centimeter.

optical measurements are acquired. The optical fiber assembly is then removed and 11 x-ray projections are taken (the breast remains in the same position and compression). The whole data collection takes 1.5 min, and the optical data and x-ray data are precisely coregistered. The optical imaging data are calibrated by use of homogeneous phantoms before and after each patient measurement.

A slice of the 3-D x-ray image from our 65-year-old patient is shown in Fig. 6. A vague density is seen in the upper outer quadrant of the left breast of this patient. After undergoing an excisional biopsy, pathology showed it to be an invasive carcinoma. The malignant region shown in this figure is the densest part of the lesion, measuring approximately  $1.0\text{ cm} \times 0.9\text{ cm}$ , circled by a thick solid line. Outside this area, multiple branches of the disease spreading to normal tissue can easily be seen, circled by a light solid line. The breast was compressed to a thickness of 6.2 cm. The source and detector positions are shown by the circles and squares, respectively, in Fig. 6 with the sources at  $z = 0\text{ cm}$  and the detectors at  $z =$

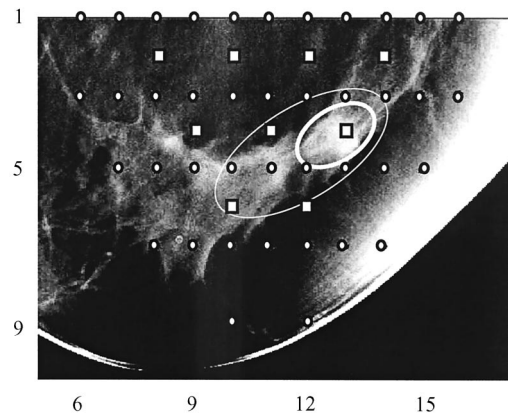


Fig. 6. Slice ( $z = 3.6\text{ cm}$ ) of the 3-D x-ray image from the patient. The circles indicate the positions of the 40 sources and the squares indicate the positions of the nine detectors. The lesion is indicated by the thick dark line with diffuse extension indicated by the thin dark line. The field of view is  $12\text{ cm} \times 9\text{ cm}$ .

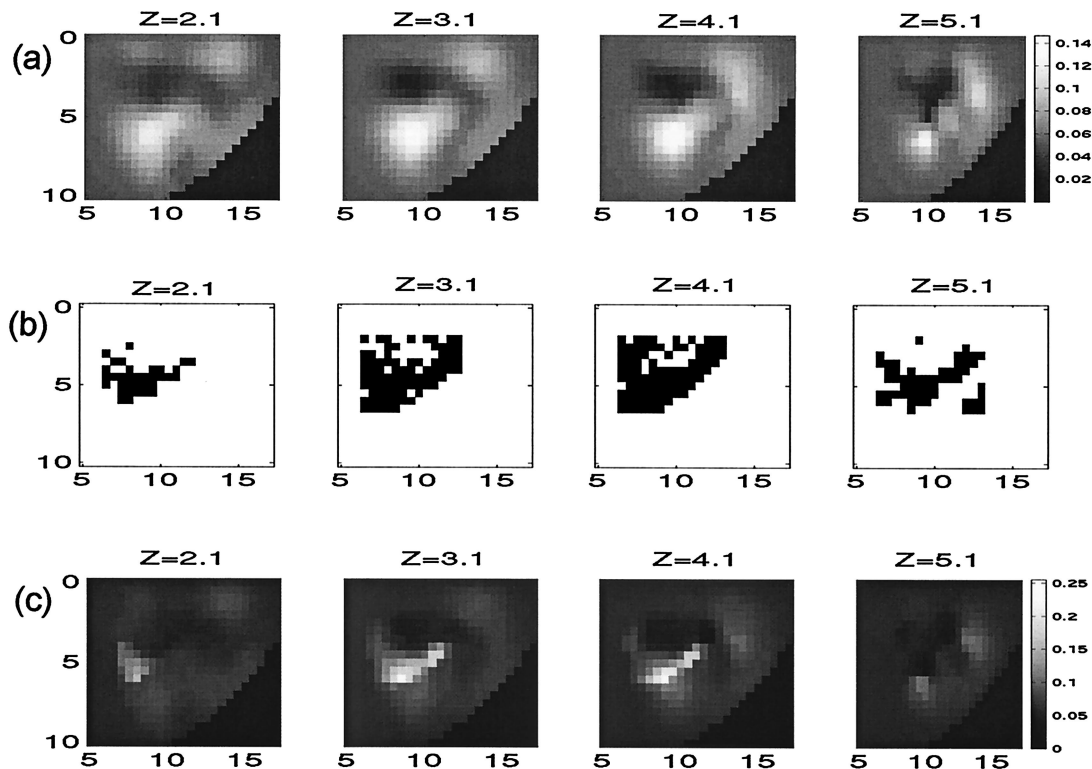


Fig. 7. (a) Absorption image reconstruction of the clinical data by use of conventional Tikhonov regularization. (b) The 3-D x-ray images after a threshold was assigned to define the spatial prior. The black voxels indicate the regions suspected of having a lesion. (c) The reconstruction of the clinical data by use of the spatial prior from (b) for regularization.

6.2 cm. The optical image is reconstructed only within the breast tissue within the entire region revealed in Fig. 6.

We retrieved the x-ray spatial prior from the x-ray images by assigning a threshold [see Fig. 7(b)]. For the background optical properties the reduced scattering coefficient was  $7.0 \text{ cm}^{-1}$  and the absorption coefficient was  $0.05 \text{ cm}^{-1}$ . The optical image without the spatial prior is shown in Fig. 7(a) ( $\alpha_1 = \alpha_2 = 0.0075$ ). This optical image shows a laterally extended increased absorption in the region of contrast identified in the x-ray image and does not resolve the contrast in the axial direction. A region of reduced absorption is noted above the lesion closer to the chest wall that corresponds with the reduced contrast observed in the x-ray image.

The image reconstructed with the spatial prior is shown in Fig. 7(c). For the regularization parameters we used values of  $\alpha_1 = 0.0075$  and  $\alpha_2 = 0.00065$  as determined by the L curve and optimal CNR procedure described for the simulations above and shown in Figs. 8(a) and 8(b). Here we see that the lesion is reconstructed with better lateral and axial resolution and that it exhibits a greater absorption relative to the background. It is interesting to note that the more sharply resolved optical contrast is not centered on the main lesion identified in the x-ray image by the thick solid line in Fig. 6 but is shifted down and to the left still within the diffuse part of the lesion. More importantly, the reconstructed optical

absorber is confined to a volume significantly smaller than the x-ray spatial prior, suggesting that the optical image is not just an artifact of the spatial prior. In contrast, when we use the original optical image [Fig. 7(a)] to produce a spatial prior as shown in Fig. 9(a), the new spatially constrained optical image [Fig. 9(b)] is strongly correlated with the spatial prior. Figure 9(b) was produced with the spatial prior shown in Fig. 9(a) with  $\alpha_1 = 0.0075$  and  $\alpha_2 = 0.0019$  (chosen by maximization of the CNR as described above). As expected, Fig. 9(b) has the same spatially structure as Fig. 7(a) since no new spatial information was provided, but has an improved spatial resolution in agreement with the simulation results shown in Figs. 1(b) and 1(d). Using the x-ray image as a spatial prior has the potential to provide new spatial information that then results in a quantitatively different image. A more thorough study of multiple lesions is required to determine whether the x-ray image as a spatial prior produces quantitatively more accurate images or on the other hand produces image artifacts.

It is possible that the reconstructed lesion is an artifact that results from a mismatch in the x-ray spatial prior and the optical contrast. We thus varied the spatial prior to examine the effect it had on the reconstructed image. First, we increased the volume of the spatial prior as shown in Fig. 10(a). The resultant image shown in Fig. 10(b) is not significantly different from that shown in Fig.

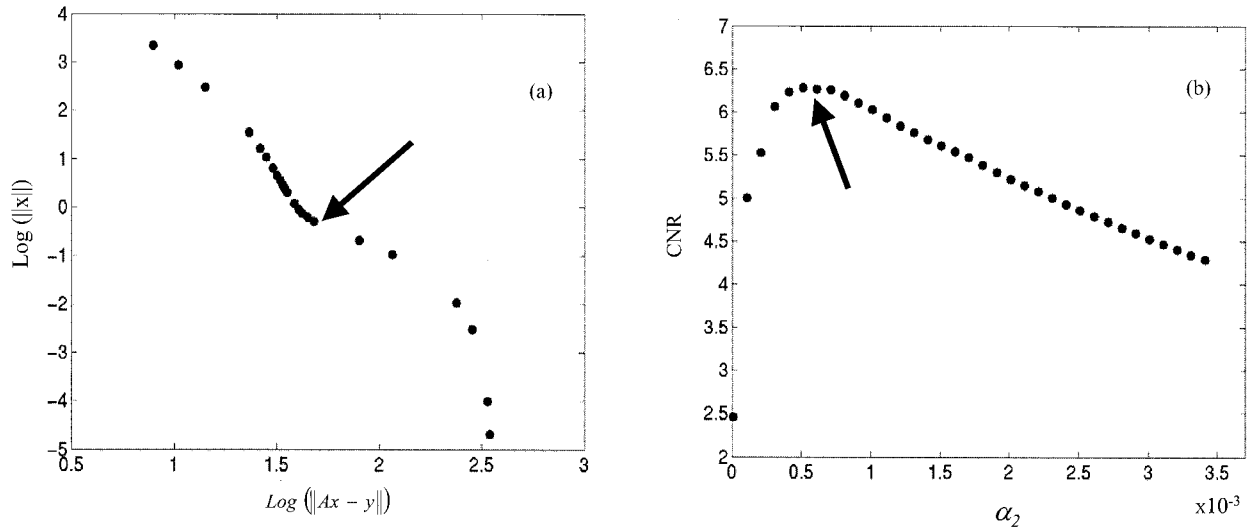


Fig. 8. (a) Plot of the L curve for the clinical image shown in Fig. 7(a). Here  $\alpha_2$  has the same value as  $\alpha_1$ . The arrow in the graph points to the L corner. (b) CNR versus  $\alpha_2$ .  $\alpha_1 = 0.0075$  remains constant at the value determined in (a). The arrow points to the maximum CNR.

7(c). We also tried an artificial spatial prior in a different region of the breast by placing a 4-cm-diameter sphere centered at  $(x, y, z) = (12, 4, 3.1)$ , 2 cm above and 2 cm to the right of the real lesion. The reconstruction from this incorrect spatial prior is shown in Fig. 11 and reveals a biased image that clearly resembles artifacts with large positive and negative amplitude variations. For this reconstruction the optimal  $\alpha_2 = 0.001$ . The magnitude of the contrast at  $(9, 6, 3.1)$  cm is comparable with that we obtained when no spatial constraint was used. When we used a spatial low-pass filter on the image with the incorrectly positioned ROI (Fig. 11), the noise in the ROI was reduced, the optical contrast at  $(9, 6, 3.1)$  cm became more apparent, and the image closely resembled the original image without a spatial prior [Fig 7(a)].

## 7. Summary

We have shown through a simulation study that spatial information provided by another imaging modality (such as x-ray tomosynthesis, x-ray computed tomography, or MRI) can be used as a prior in the diffuse optical image reconstruction to improve the image contrast-to-noise ratio and resolution. In addition, we demonstrated a dramatic improvement in image resolution for clinical tomographic optical breast imaging data guided by a 3-D x-ray tomosynthesis. We used the prior spatial information to determine the form of the spatial regularization of the diffuse optical inverse problem as implemented by a modification of the Tikhonov regularization. We used the spatial prior to define a two-valued regularization function and showed that the two regulariza-

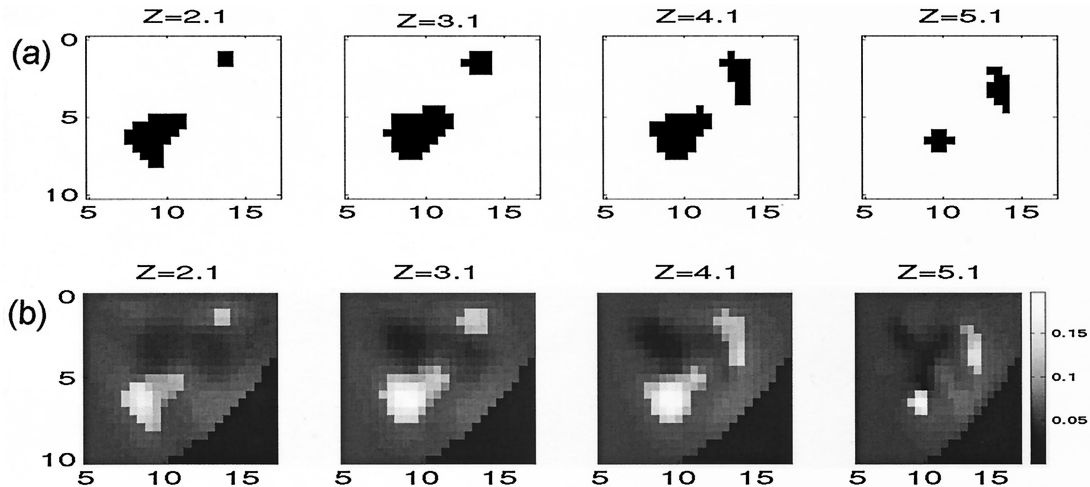


Fig. 9. (a) Spatial prior defined from a threshold of the original optical image in Fig. 7(a). (b) The reconstructed absorption image using (a) as the spatial prior. The image units are in reciprocal centimeters. The field of view of the image is 12 cm  $\times$  10 cm, and image slices are shown every centimeter.

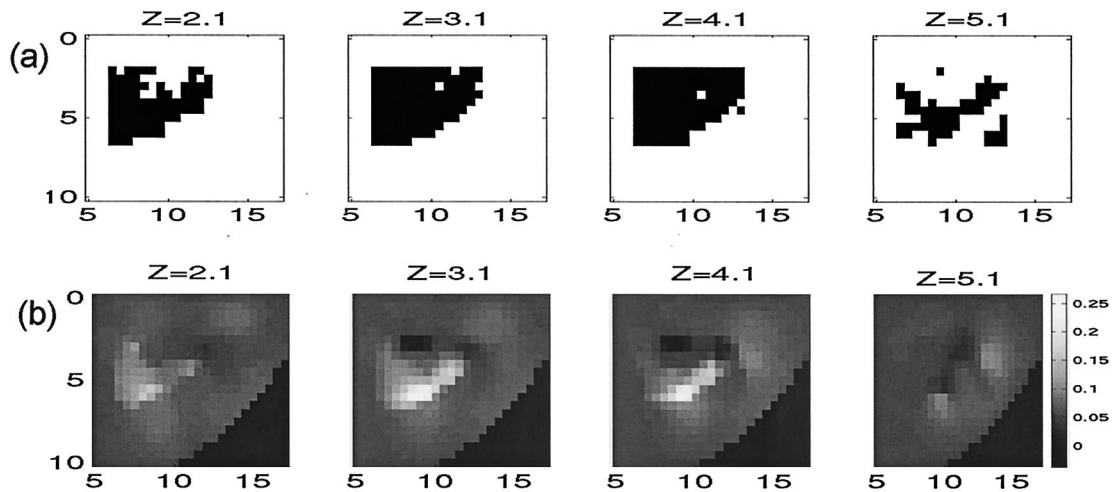


Fig. 10. (a) Larger volume 3-D spatial prior derived by use of a lower threshold on the x-ray image. (b) Image reconstruction by use of the larger volume spatial constraint.

tion values could be determined objectively and without knowledge of the true solution by implementing the standard L-curve technique and maximizing the image CNR. We could, in general, have a continually varying regularization function derived by some linear (or nonlinear) function of the spatial prior, but this would require more confidence in the relationship between the spatial prior and the optical absorption and scattering properties of the tissue. More knowledge of this relationship will be obtained in the future as more multimodality, coregistered imaging is performed.

The results presented here are for reconstruction of absorption images but the same framework can be used to image the scattering coefficient. Imaging simultaneously the absorption and the scattering coefficients will introduce a third regularization parameter ( $\alpha_3$ ). A method for choosing the three optimal regularization parameters will have to be explored, but perhaps maximization of the image CNR surface as a function of  $\alpha_2$  and  $\alpha_3$  will suffice.

The purpose for using a spatial prior as a soft structural constraint rather than a hard structural constraint is to indicate an increased likelihood of optical contrast in a region of interest rather than to force the reconstruction of optical contrast in that region. Such a soft structural constraint does have the potential to bias the image if the constraint is inconsistent with the data. On the other hand, a hard

structural constraint will certainly bias the image if it is inconsistent with the data. Our simulation results indicate that image bias will occur when the spatial prior has a small inconsistency with the data, but a large inconsistency will not produce image bias. The image bias was also observed in the clinical results when a fake spatial prior was constructed. The bias in this case, however, was obvious as large, unphysical, amplitude fluctuations were observed to occur within the region of interest and could be easily removed by a spatial low-pass filter of the image.

In the absence of a spatial prior provided by another imaging modality, such as x ray or MRI, one could use the original optical image to define the spatial prior. This does improve the spatial resolution of the resultant image in a way similar to the zonation procedure followed by Eppstein *et al.*,<sup>26</sup> but it does not incorporate new spatial information into the image reconstruction. Further research with larger sets of multimodality breast imaging data is required to determine if the additional spatial information provided by x ray or MRI can be utilized as a spatial prior to improve the optical image as described here. Finally, future studies could attempt to incorporate spectral priors with these spatial priors to improve image quality further and perhaps to improve specificity between malignant and benign lesions.

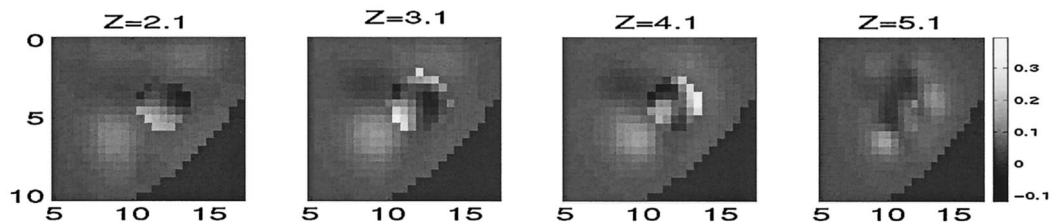


Fig. 11. Absorption image reconstruction of clinical data by use of an artificial spatial prior (image units are in reciprocal centimeters). The field of view of the image is 12 cm  $\times$  10 cm, and image slices are shown every centimeter.

D. A. Boas acknowledges funding from Advanced Research Technologies, NIH R29-NS38842, NIH P41-RR14075, and NIH R01-CA97305, and from the Center for Innovative Minimally Invasive Therapies. This research was funded in part by the U.S. Army under Cooperative Agreement DAMD17-99-2-9001. The material presented does not necessarily reflect the position or the policy of the Government, and no official endorsement should be inferred. This research was supported in part by CenSSIS, the Center for Subsurface Sensing and Imaging Systems, under the Engineering Research Centers Program of the National Science Foundation (award EEC-9986821). The authors thank the reviewers for suggesting the use of the original optical image as a spatial prior.

## References

1. A. Yodh and B. Chance, "Spectroscopy and imaging with diffusing light," *Phys. Today* **48**, 34–40 (1995).
2. S. R. Arridge, "Optical tomography in medical imaging," *Inverse Probl.* **15**, R41–R93 (1999).
3. D. A. Boas, D. H. Brooks, E. L. Miller, C. A. DiMarzio, M. Kilmer, R. J. Gaudette, and Q. Zhang, "Imaging the body with diffuse optical tomography," *IEEE Signal Process. Mag.* **18** (6), 57–75 (2001).
4. Y. Hoshi and M. Tamura, "Near-infrared optical detection of sequential brain activation in the prefrontal cortex during mental tasks," *Neuroimage* **5**, 292–297 (1997).
5. A. Maki, Y. Yamashita, E. Watanabe, and H. Koizumi, "Visualizing human motor activity by using non-invasive optical topography," *Front. Med. Biol. Eng.* **7**, 285–297 (1996).
6. B. Chance, A. Endla, N. Shoko, Z. Shuoming, H. Long, K. Worden, C. Li, T. Murray, Y. Ovetsky, D. Pidikiti, and R. Thomas, "A novel method for fast imaging of brain function, non-invasively, with light," *Opt. Express* **2**, 411–423 (1998), <http://www.opticsexpress.org>
7. M. A. Franceschini, V. Toronov, M. Filiaci, E. Gratton, and S. Fanini, "On-line optical imaging of the human brain with 160-ms temporal resolution," *Opt. Express* **6**, 49–57 (2000), <http://www.opticsexpress.org>.
8. S. R. Hintz, D. A. Benaron, A. M. Siegel, A. Zourabian, D. K. Stevenson, and D. A. Boas, "Bedside functional imaging of the premature infant brain during passive motor activation," *J. Perinat. Med.* **29**, 335–343 (2001).
9. J. P. Culver, V. Ntziachristos, M. J. Holboke, and A. G. Yodh, "Optimization of optode arrangements for diffuse optical tomography: a singular-value analysis," *Opt. Lett.* **26**, 701–703 (2001).
10. R. L. Barbour, H. L. Graber, J. Chang, S. S. Barbour, P. C. Koo, and R. Aronson, "MRI-guided optical tomography: prospects and computation for a new imaging method," *IEEE Comput. Sci. Eng.* **2**(4), 63–77 (1995).
11. V. Ntziachristos, A. G. Yodh, M. Schnall, and B. Chance, "MRI-guided diffuse optical spectroscopy of malignant and benign breast lesions," *Neoplasia* **4**, 347–354 (2002).
12. Q. Zhu, T. Durduran, V. Ntziachristos, M. Holboke, and A. G. Yodh, "Imager that combines near-infrared diffusive light and ultrasound," *Opt. Lett.* **24**, 1050–1052 (1999).
13. M. A. O'Leary, "Imaging with diffuse photon density waves," Ph.D. dissertation (Department of Physics, University of Pennsylvania, Philadelphia, Pa., 1996).
14. B. W. Pogue, T. O. McBride, J. Prewitt, U. L. Osterberg, and K. D. Paulsen, "Spatially variant regularization improves diffuse optical tomography," *Appl. Opt.* **38**, 2950–2961 (1999).
15. O. Arıkan, "Regularized inversion of a two-dimensional integral equation with applications in borehole induction measurements," *Radio Sci.* **29**, 519–538 (1994).
16. M. Belge, M. Kilmer, and L. E. Miller, "Efficient determination of multiple regularization parameters in a generalized L-curve framework," *Inverse Probl.* **18**, 1161–1183 (2002).
17. S. R. Arridge and M. Schweiger, "Inverse methods for optical tomography," in *Proceedings of Information Processing in Medical Imaging (IPMF93)*, H. H. Barrett and A. F. Gmitro, eds., Vol. 687 of Lecture Notes in Computer Science, (Springer-Verlag, New York, 1993).
18. S. R. Arridge, "Photo-measurement density functions. Part I: Analytical forms," *Appl. Opt.* **34**, 7395–7409 (1995).
19. D. A. Boas, "Diffuse photon probes of structural and dynamical properties of turbid media: theory and biomedical applications," Ph.D. dissertation (Department of Physics, University of Pennsylvania, Philadelphia, Pa., 1996).
20. R. J. Gaudette, D. H. Brooks, C. A. DiMarzio, M. E. Kilmer, E. L. Miller, T. Gaudette, and D. A. Boas, "A comparison study of linear reconstruction techniques for diffuse optical tomographic imaging of absorption coefficient," *Phys. Med. Biol.* **45**, 1051–1070 (2000).
21. Q. Zhang, T. J. Brukilacchio, T. Gaudett, L. Wang, A. Li, and D. A. Boas, "Experimental comparison of using continuous-wave and frequency-domain diffuse optical imaging systems to detect heterogeneities," in *Optical Tomography and Spectroscopy of Tissue IV*, B. Chance, R. R. Alfano, B. J. Tromberg, M. Tamura, E. M. Sevick-Muraca, Proc. SPIE **4250**, 219–238 (2001).
22. P. C. Hansen, *Rank-Deficient and Discrete Ill-Posed Problems: Numerical Aspects of Linear Inversion* (SIAM Press, Philadelphia, Pa., 1998).
23. J. P. Culver, R. Choe, M. J. Holboke, L. Zubkov, T. Durduran, A. Slemple, V. Ntziachristos, B. Chance, and A. G. Yodh, "Three-dimensional diffuse optical tomography in the parallel plane transmission geometry: evaluation of a hybrid frequency domain/continuous wave clinical system for breast imaging," *Med. Phys.* **30**, 235–247 (2003).
24. L. T. Niklason, B. T. Christian, L. E. Niklason, D. B. Kopans, D. E. Castleberry, B. H. Opsahl-Ong, C. E. Landberg, P. J. Slanetz, A. A. Giardino, R. Moore, D. Albagli, M. C. DeJule, P. E. Fitzgerald, D. F. Fobare, B. W. Giambattista, R. F. Kwasnick, J. Liu, S. J. Lubowski, G. E. Possin, J. F. Richotte, C.-Y. Wei, and R. F. Wirth, "Digital tomosynthesis in breast imaging," *Radiology* **205**, 399–406 (1997).
25. T. Wu, "Three dimensional mammography reconstruction using low dose projection images," Ph. D. dissertation (Department of Physics, Brandeis University, Waltham, Mass., 2002).
26. M. J. D. Eppstein, D. E. Troy, T. L. Troy, and E. M. and Sevick-Muraca, "Biomedical optical tomography using dynamic parameterization and Bayesian conditioning on photon migration measurements," *Appl. Opt.* **38**, 2138–2150 (1999).